International Journal of Combinatorial Optimization Problems and Informatics, 14(1), Jan-April 2023, 39-48. ISSN: 2007-1558.

www.editada.org

Dendritic neural networks in the classification of estrous cycle images

Rocio Ochoa-Montiel[1,2], Rodrigo Román-Godínez[1], Erik Zamora[1], Humberto Sossa[1,3], and Gerardo Hernández[4]

[1] Instituto Politécnico Nacional - CIC, Av. Juan de Dios Batiz S/N, Gustavo A. Madero, 07738 México City, México.
[2] Universidad Autónoma de Tlaxcala, Facultad de Ciencias Básicas, Ingeniería y Tecnología, Tlaxcala, México.
[3] Tecnológico de Monterrey, Campus Guadalajara. Av. Gral. Ramón Corona 2514 Zapopan, Jalisco. 45138, México.
[4] Universidad Autónoma de la Ciudad de México, Colegio de Ciencia y Tecnología, Ciudad de México, México.
{ma.rocio.ochoa, rodrigo0045, humbertososa, gerardohernandez.hernandez}@gmail.com, ezamora@ipn.mx

Abstract. In the biological area, the short reproductive cycle in rodents is useful because it allows analyzed electrophysiological properties, behaviors, or drug effects through the changes observed during this period. This cycle is composed of 4 stages in which the classification is determined by vaginal cytology.
Although automatic approaches have been used for the classification of these stages, they are computationally expensive and require a great number of images for adequate performance.
In this paper, we test different models of dendritic neural networks (DNN) trained by stochastic gradient descent to classify a short number of images and four classical contrast enhancement methods. We extract texture features and use standard and DNN classifiers to recognize the images.
From the experiments, it seems that DNNs have a more stable behavior concerning the standard classifiers according to the standard deviation presented, being this a desirable property for a model. We consider that DNN could be an adequate alternative for the classification of estrous cycle images.

Keywords: Dendrite neural networks· Multi-Layer Perceptron· Estrous cycle.

Article Info
Received Sep 30, 2022
Accepted Jan 20, 2023

1 Introduction

Computational vision is applied in different areas [1,2,3]. In Biology, the analysis of rodent tissues is useful to study physiological processes because these are carrying on short periods. The reproduction is an ideal process for researching changes along a cycle, such as fertility rates, effects of treatments, or environmental diverse conditions, among others [4,5]. The reproductive cycle in rodents is named Estrous cycle, it is formed by four phases: proestrus P, estrus E, metestrus M and diestrus D. Knowledge of these stages is important for interpretations of female animals' data, whereas their identification is through the observation of cells in vaginal smears where properties like type, number, shape, size, and proportion of cells are evaluated [6,7]. However, recognition is a manual task performed by an expert, so the analysis is subjective due to the

particular skills of each examiner. Furthermore, the analysis is time consuming. Thus, computational vision techniques are helpful to address the automatic recognition problem of estrous cycle.

One aspect that has influenced the low use of these techniques is the scarce amount of correctly labeled data for an adequate validation of the models. Proposals found so far include a quantitative method for assessing Estrous cycle stages [8]. However, the method focuses on showing trends between diverse cell types in each stage. A proposal that enables more efficient cycle stage data analysis and pattern visualization is propose in [9], while in [10] the visual classification of the estrous cycle images is addressed by using support vector machines, multilayer perceptron networks, and convolutional neural networks [11]. On the other hand, neural networks with dendritic processing have been used in recent years to solve different classification problems [12,13,14]. The main feature of dendritic neural networks (DNNs) is that they generate closed decision boundaries with a single processing unit [15,16,17,18], which is useful for solving nonconvex problems without hidden layers. This simplicity represents an advantage over CNNs due to the computational savings involved. In [19,20], these networks use the fusion of linear units and a type of DNN as a form of hybrid network.

In this work, for the first time, we evaluate the performance of dendritic neural networks on the classification of estrous cycle images from texture features. These features have been selected due to their rotation, scale, and translation invariance properties. It is important to mention that our objective is to know the impact of these models for pattern classification in data sets for a problem that has been little explored, and not to exceed the classification rate of previous works [10,11]. In the next section, the materials and methods are described. Section 3 presents the proposed methodology. In section 4, experiments and results are shown. Conclusions are included in section 5.

2 Materials

In this section, we provide the theoretical concepts that support this research work. First, we describe the methods applied to the data for the construction of the datasets used in the experiments. Subsequently, the general characteristics of the classifiers evaluated are described.

2.1 Contrast enhancement methods

The simplest kinds of image processing are point methods, where each output pixel value depends on an input pixel value; including some globally recovered information or parameters. Common techniques of image enhancement as histogram equalization (HE), adaptive histogram equalization (AHE), and local saturation (LS) are in this category. We decided to use these because the aim is to enhance details over small or regular areas in the images [21].

HE enhances the contrast of images by transforming the values in an intensity image so that the histogram of the output image approximately matches a specified histogram, uniform distribution by default. Whereas, AHE performs contrast-limited adaptive histogram equalization. Unlike HE, it operates on small data regions (or tiles) rather than the entire image. On the other hand, LS increases the image contrast by mapping the values of the input intensity image to new values, hence n% of the data is saturated at low and high intensities of the input data. Furthermore, we use an automatic contrast enhancement (ACE) proposed in previous work [22], which enhances the contrast on local areas through a histogram approximation using differential evolution. An advantage of this method is the possibility of defining in which areas of the image we want to contrast enhancement. Thus, clearer or darker regions (Cr or Dr) can be selected for the enhancement.

2.2 Classifiers

Most classifiers used in machine learning require features extracted previously in a manual or semi-automatic way. Classifiers as multilayer perceptron (MLP), random forest (RF), and the smooth dendrite morphological neurons (SDMN) are of this type. The firsts are known for their good performance in diverse applications, whereas the SDMN is a last generation net recently proposed by [23] that has a good generalization capacity.

Convolutional neural networks (CNNs) are the most representative approach for automatic classification due to they automatically extract features and perform classification. These models do not need previous image processing or explicit feature extraction. Instead, they use the image to find adequate descriptors for image classification. It is assumed that learning occurs by using patterns directly from the input image data exclusively, without considering previous knowledge.

Dendritic neural networks (DNN) are neural classifiers that can enclose patterns on a closed decision boundary with only one neuron. The Dendritic morphological neuron (DMN) creates a hyper box by finding the values for two opposite vertexes, and it uses lattice algebra operators like min, max, addition, and subtraction [15,24]; the classification performance of this net is evaluated and improved in [25]. In addition, there are hybrid models with DMN and linear neurons [18,19,20]. Another DNN is the Dendritic ellipsoidal neuron which uses the Mahalanobis distance to determine the decision boundary to enclose the patterns into a hyper ellipsoid [21]. As a simplification of this model, a dendritic spherical neuron that only uses the centroid and radius to classify the pattern is proposed in [22]; and a combination of DEN-perceptron and DSN-perceptron is proposed in [23] as a new hybrid architecture for classification.

2.3 Dendritic Morphological Neuron

Dendritic Morphological Neuron (DMN) segments the input space into hyperboxes of N dimensions where $N \in I^+$. After processing the data, the output $d_c(x)$ is given by the equations (1) and (2):

$$d_c(x) = \underset{c}{argmax}\left(h_{k,c}(x)\right) \tag{1}$$

$$h_{k,c}(x) = \underset{2}{min}\left(\underset{N}{min}\left(x_i - w_{min}, w_{max} - x_i\right)\right), i = \{0,1,2,\dots n\} \tag{2}$$

Here, $h_{k,c}(x)$ is the output of a dendrite, k indicates a specific dendrite and $k \in I^+$, c represents the class and $c \in I^+$, x is an input vector and $x \in N$, w_{min} and w_{max} are the weight vectors that represent the opposite vertices of the hyperbox, If $h_{k,c} \geq 0$, it belongs to the class, otherwise, it does not belong to it as it shows Figure 1.

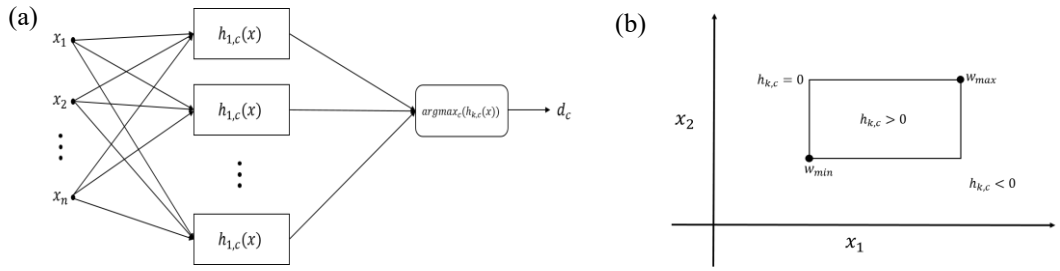

Figure 1. (a) Architecture of Dendrite Morphological Neuron. (b) Example of an hyperbox in 2D.

2.4 Dendrite Ellipsoidal Neuron

This neuron uses the Mahalanobis distance to determine if the output τ_j belongs to a class or not, where :

$$\tau_j = argmin_k\left(\tau_j^k\right) \tag{3}$$

$$\tau_k^j = (x_i - \mu_k)^T \sum_k^{-1} (x_i - \mu_k) \tag{4}$$

Here, τ_j^k is the output of a dendrite, μ_k is a mean vector, and $\sum_k^{-1}$ is a covariance matrix and associated with the k-th cluster, $K = 1,\dots,k$, and x_i is the input pattern. A pattern is assigned to the class whose

dendrite output outputs the minimum distance that is ff $h_{k,c} < 0$, then the input or if $h_{k,c} = 0$, otherwise, it is declared to be outside of the class as it shows Figure 2.

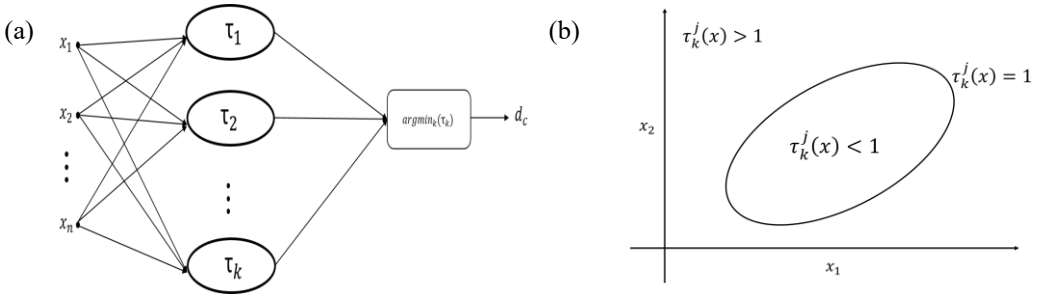

Figure 2. (a) Architecture of Dendrite Ellipsoidal Neuron. (b) Example of an hyperellipsoid in 2D

2.5 Dendrite Spherical Neuron

DSN compares the distance of every input data to the center of the hypersphere against its radius as it shows the equations (5) and (6):

$$d_j(x) = max\left(h_{i,j}(x)\right), i = 1, \dots l_j \tag{5}$$

$$h_{i,j}(x) = r_{i,j} - \left\|x - c_{i,j}\right\|^2 \tag{6}$$

Where, $\|*\|$ is the Euclidean norm. $c_{i,j} \in R^D$ is the centroid of the dendrite, and r is the radius. If $h_{i,j}(x) < 0$ we say that the input does not belong to the class. However, if a number greater or equal to zero is obtained, it means that the pattern belongs to the class, as it shows Figure 3.

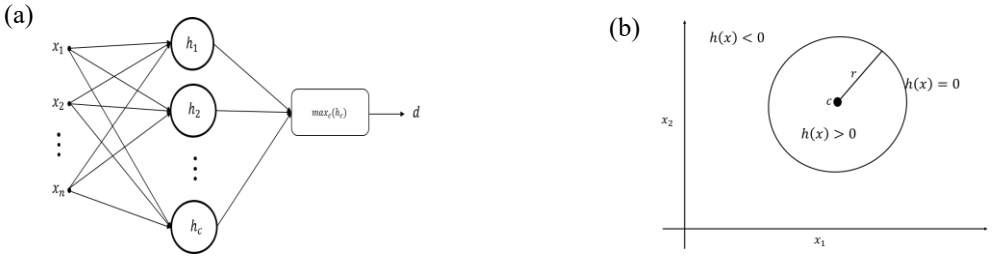

Figure 3. (a) Architecture of Dendrite Spherical Neuron. (b) Example of a hyperspheres in 2D

2.6 Hybrid architectures

From the above three neurons combine with a classical perceptron we get 6 different models, two of them, morphological-linear neural network and linear-morphological neural network proposed by G. Hernandez [19], and another four inspired in these two model by changing the dendrite part by DSN or DEN architectures. To include all of them, we are going to refer to the name of dendrite-linear neural networks and linear-dendrite neural networks.

2.6.1 Dendrite-linear neural networks

The first part of this architecture is a dendrite processing that could be either DMN, DEN or DSN dendrite neural networks as feature extractor and then a perceptron layer as an output with a sigmoid function for bi-classes problems and softmax layer for multi-class problems. Thus, we can define the model with:

$$Y(x) = \rho(\sum_{i=1}^{k}(w_i f_i(\boldsymbol{x}) + b)) \tag{7}$$

Where $f_i(x)$ is one of the outputs of equations: 2, 4, or 6 with $tanh$ as activation function; i is the number of dendrites and ρ is the activation function that fits the problem. In figure 4 we can see the tree kinds of hybrid neurons for multiclass classification.

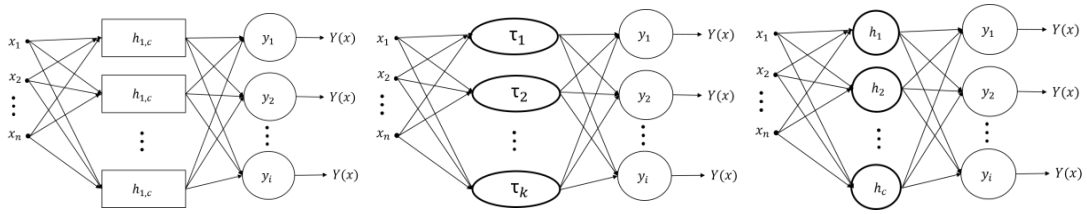

(a) (b) (c)

Figure 4. (a)Architecture of a DMN-Linear neuron, (b)Architecture of a DEN-Linear neuron and (c)Architecture of a DSN-Linear neuron

2.6.2 Linear-dendrite neural networks

For this second architecture we change the order of the unit, using a layer of perceptron as feature extractor and then dendrites unit as output layer with a sigmoid function for bi-classes problems and softmax layer for multi-class problems. Thus, we can define the model with:

$$y_i(x) = \boldsymbol{W^t}\, \boldsymbol{x} + \boldsymbol{b}_i \tag{8}$$

$$Y_c(x) = f(y_i) \tag{9}$$

Where y_i is the output of the perceptron layer, W is a matrix of weights, $\boldsymbol{b_i}$ is a vector of bias; $Y_c(x)$ is the output of the hybrid neuron $f(y_i)$ is a layer of one of de dendrites models, could be equation 2, 4 or 6 with a sigmoid as activation function for bi-class classification and softmax for multi-class classification. In figure 5 we can see the tree kinds of hybrid neurons for multiclass classification.

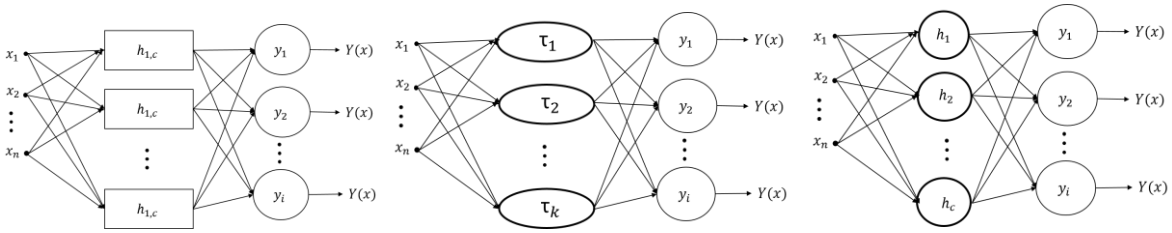

(a) (b) (c)

Figure 5. (a)Architecture of a Linear-DMN neuron, (b)Architecture of a Linear-DEN neuron and (c)Architecture of a Linear-DSN neuron

3 Methodology

In this work we use a balanced dataset of 344 images with 86 for each stage of the estrous cycle. Images were acquired with an optical microscope using a magnification of 400X and a camera Logitech C170. These images are in .jpg format with a resolution of 100 ×90 [26]. From the dataset, we use the G band images because this shows better contrast concerning the R and B bands. Datasets used in the experiments are built applying the contrast enhancement methods ACE (Cr, and Dr), HE, AHE, and LS. ACE was implemented according to [22], and the methods remainder are computed with the functions histeq, adapthisteq, and imadjust, respectivetly from the image processing toolbox of Matlab with the default parameters for these

functions. Additionally, a dataset is built from the images of band G without applying contrast enhancement. In this way, we obtain six datasets for the experiments. **Error! Reference source not found.** shows the images obtained from the methods applied.

Figure 6. Images of datasets used. Row 1. Band G, row 2. ACE (Cr), row 3. ACE (Dr), row 4. HE, row 5. AHE, and row 6. LS.

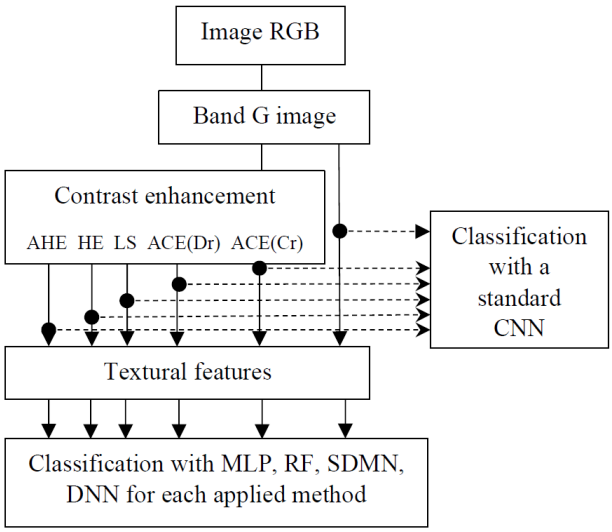

Figure 7. General flowchart of the proposed methodology

First, we apply the contrast enhancement methods mentioned in the previous section. In addition, we consider images without applying the contrast enhancement to compare. After that, textural features based on the gray level co-occurrence matrix (GLCM) are extracted. These features are used by the classifiers MLP, RF, SDMN and, DNN. On the other hand, to compare with an automatic classification method, we use a CNN. Finally, we assessment the classification performance for each image class P, E, M, and D, which depict the four phases of the estrous cycle. To test the classifiers MLP, RF, SDMN, and DNN we use textural features since the images are in grayscale; whereas CNN uses the images directly. Figure 7 shows the general flowchart of the proposed methodology.

The textural features for the experiments are computed from the gray level-co-occurrence using eight gray levels. Because the GLCM probabilities represent the conditional joint probabilities of all pairwise combinations of gray levels in the spatial windows of interest given the parameters interpixel distance (δ) an orientation (θ), we adjust $\delta = 1$, and $\theta = \{0, 45, 90, 135\}$.

We use seven shift-invariant features suggested by [27]: uniformity, entropy, dissimilarity, inverse difference, inverse difference moment, and correlation. These features are computed for each value of θ. Later, we average the four interpixel orientations for each feature, thus we obtain seven features for each image. These features are used independently by each classifier. For the MLP, we consider one hidden layer with 50 neurons and the activation function traingdx from the Matlab toolbox. These parameters were obtained by experimentation. RF was initialized with 500 trees and the classification is performed by majority vote as in [28]. SDMN was used with the parameters suggested in [23]. On the other hand, for DNN and hybrid neurons, we performed a grid search for hyper parameter tuning to evaluate from four to a hundred dendrites, with the optimizers: RMSprop, SGD and Adam, and tanh as activation function to handle negative values.

4 Experiments and Results

The experiments were performed on a CPU i9, 64GB RAM, Windows10, graphics processing unit (GPU) GeForceGTX 1080, Matlab and phyton.

For the experiments with the CNN, we use a structure composed by four convolutional and max-pooling layers. The feature maps are flattened and reduced to an output of size four. Data augmentation is used on the training set. The augmentation operations include horizontal and vertical reflexion. Accordingly, we have the addition of a random number of augmented images to the training set in each epoch. The number of filters in the four convolutional layers are 4, 8, 16, and 32. The training process is stopped when the validation loss does not decrease for 20 epochs. In all experiments, we use 50% of data for training, 20% for validation, and the remainder for testing. Five-fold cross-validation is used to assess the training performance, and the best net model from the five-fold validation is selected and used with the test set to assess the net performance. To evaluate the global classification performance, we repeat the experiment ten times.

Table 1 Accuracy of classifiers SDMN, MLP, RF, and CNN

Method	**SDMN %**		**MLP %**		**RF %**		**CNN %**	
Band G	62.50	±3.55	69.23	±4.04	64.42	±2.82	68.27	±4.26
AHE	68.33	±4.88	70.19	±3.91	61.54	±1.78	62.50	±7.74
HE	61.67	±3.01	53.85	±3.04	55.77	±2.43	49.04	±9.27
LS	69.17	±5.18	67.31	±2.80	69.23	±3.43	58.65	±5.04
ACE (Dr)	69.17	±4.90	63.46	±1.50	61.54	±2.87	48.08	±5.64
ACE (Cr)	71.25	±4.49	67.31	±3.71	61.54	±2.02	48.08	±8.19
Mean	67.02	±4.34	65.23	±3.17	62.34	±2.56	55.77	±6.69
Min	61.67	±3.01	53.85	±1.50	55.77	±1.78	48.08	±4.26
Max	71.25	±5.18	70.19	±4.04	69.23	±3.43	68.27	±9.27

Results of classification experiments for the datasets—Band G, AHE, HE, LS, ACE(Dr), ACE(Cr)— are presented in Table 1. Note that results in ACE(Cr) reached the best performance. In general the methods in which the output image does not tend to binarization are adequate for classifying when textural features are used. On the other hand, the average by classifier shows that classifiers with better performace are SDMN and MLP, whereas the worst performance is achieved by the CNN.

Furthermore, we show in
Figure 8. Confusion matrix of the best solution. Row1: stage P, Row2: stage E, Row3: stage M, Row4: stage D the confusion matrix for the best solution (this is, accuracy=71.25 for SDMN in Table 1). We observed that the stage P is the best recognized, while the stage E obtains poor classification results.

				%Acc./class
45	1	8	6	94.11
0	55	0	5	66.66
12	1	38	9	72.22
8	10	9	33	76.47

Figure 8. Confusion matrix of the best solution. Row1: stage P, Row2: stage E, Row3: stage M, Row4: stage D

Regarding CNN, the features are automatically extracted by the net, and the contrast enhancement methods are not useful for classifying, as we can see in Table 1. Finally, it is to note that method HE shows poor performance in all tests. Experiments with DNN include the hybrid models: P-DMN, P-DSN, P-DEN, DMN-P, and DSN-P, as well as the standard DMN and DSN models. The results shown in Tables 2 and 3 show that although the performance achieved does not exceed the results of previous experiments, in all cases, the DNNs have a more consistent behavior for the previously tested methods. This can be noticed in the low average values of the standard deviation, which concerning those shown in Table 1, are significantly lower.

Of the DNN variants tested, the P-DSN model showed the best performance reaching 67.11% accuracy, as well as the lowest standard deviation relative to the other variants evaluated.

Table 2. Accuracy of experimental results of hybrid DNN

Method	**P-DMN %**	**P-DSN %**	**P-DEN**	**DMN-P%**	**DEN-P %**	**DSN-P %**
Band G	64.90 ±1.62	67.11 ±0.71	66.25 ±1.84	64.32 ±1.09	63.84 ±3.87	65.09 ±1.92
AHE	61.34 ±1.96	62.50 ±1.48	62.98 ±2.02	59.61 ±2.01	57.49 ±1.82	60.38 ±2.18
HE	48.26 ±1.59	47.88 ±1.65	49.51 ±1.78	50.86 ±2.08	47.30 ±2.91	50.67 ±1.29
LS	62.78 ±4.30	63.17 ±1.36	66.05 ±2.47	64.23 ±1.65	64.42 ±5.72	65.19 ±3.95
ACE (Dr)	61.44 ±1.69	63.36 ±1.69	54.51 ±8.33	62.30 ±1.76	58.07 ±6.79	65.38 ±1.60
ACE (Cr)	61.53 ±1.72	62.30 ±2.81	63.84 ±2.11	61.05 ±2.14	58.26 ±3.74	59.03 ±2.55
Mean	60.04 ±2.14	61.05 ±1.61	60.52 ±3.09	60.40 ±1.79	58.23 ±4.14	60.95 ±2.25
Min	48.26 ±1.59	47.88 ±1.65	49.51 ±1.78	50.86 ±2.08	47.30 ±2.91	50.67 ±1.29
Max	64.90 ±1.62	67.11 ±0.71	66.25 ±1.84	64.32 ±1.09	64.42 ±5.72	65.38 ±1.60

It is to note from the images in Figure 6, the HE contrast enhancement method produces images with high contrast, such that some regions of the images with a minimal difference in their gray levels are considered the same region. As a consequence, the texture descriptors are not suitable for correct classification in all the classifiers used. On the other hand, the low performance of CNNs can be attributed to the similarity between the distribution of gray levels in the four classes of images, and the low number of images used.

Table 3. Accuracy of experimental results of DMN and DSN

Method	DMN %	DEN %	DSN %
Band G	55.09 ±2.01	57.69 ±0.76	62.88 ±1.37
AHE	57.69 ±1.92	57.30 ±4.16	62.88 ±1.67
HE	51.73 ±1.76	48.46 ±0.76	51.25 ±1.29
LS	50.09 ±3.37	62.69 ±2.91	65.28 ±3.28
ACE (Dr)	61.34 ±2.22	55.76 ±2.46	63.26 ±1.91
ACE (Cr)	58.94 ±3.94	57.49 ±4.45	62.5 ±2.19
Mean	55.81 ±2.54	56.56 ±2.58	61.34 ±1.95
Min	50.09 ±3.37	48.46 ±0.76	51.25 ±1.29
Max	61.34 ±2.22	62.69 ±2.91	65.28 ±3.28

5 Conclusions and considerations for Future work

This work proposes use dendritic neural nets for classifying the four stages in the reproductive cycle on rodents (estrous cycle). The objective is to evaluate the performance of the DNN regard another classifiers commonly used in literature. From the results, it is worth to note that DNNs provide greater consistency relative to standard classifiers, although slightly lower performance. This is important because depicts the stable behavior of the model, which is clear from the fact that the average standard deviation for most of the dendritic networks tested was lower than for the MLP, RF, and CNN methods, except for the DEN-P network.

It is also observed that the use of contrast enhancement techniques is not relevant in the performance of DNNs, and minimally so in standard classifiers. Since the performance is low for all the classifiers evaluated, it is clear that a feature relevance analysis is required to improve the classification rate.

In future work, we like to improve the classification rate through an analysis of the features selection of images and, evaluate the performance of classifiers with larger, unbalanced datasets.

Acknowledgements

Authors would like to acknowledge the support provided by the Instituto Politécnico Nacional under projects: SIP 20210788 and 20220226; CONACYT under projects: 65 (Fronteras de la Ciencia) and 6005 (FORDECYT-PRONACES). First author thanks the Autonomous University of Tlaxcala, Mexico for the support. Authors also express their gratitude to the Applied Computational Intelligence Network (RedICA).

Referencias

1. G. Chen et al. (2021) "A Novel Illumination-Robust Hand Gesture Recognition System With Event-Based Neuromorphic Vision Sensor," in IEEE Transactions on Automation Science and Engineering, vol. 18, no. 2, pp. 508-520, doi: 10.1109/TASE.2020.3045880.
2. L. R. Kennedy-Metz *et al*. (2021) "Computer Vision in the Operating Room: Opportunities and Caveats," in *IEEE Transactions on Medical Robotics and Bionics*, vol. 3, no. 1, pp. 2-10, doi: 10.1109/TMRB.2020.3040002.
3. F. Baghaei Naeini *et al*. (2020)"A Novel Dynamic-Vision-Based Approach for Tactile Sensing Applications," in *IEEE Transactions on Instrumentation and Measurement*, vol. 69, no. 5, pp. 1881-1893, doi: 10.1109/TIM.2019.2919354.
4. Priddy, B. C. (2016). Sex, strain, and estrous cycle influences on alcohol drinking in rats. *Pharmacology Biochemistry and Behavior*, 61-67.
5. Kaur, S. B. (2018). Sex differences and estrous cycle effects of peripheral serotonin-evoked rodent pain behavioors. *Neuroscience*, 87-100.

6. Byers, S. W. (2012). Mouse estrous cycle identification tool and images. *Plos one*.
7. Cora, M. K. (2015). Cytology of the laboratory rat and mouse: Review and criteria for the staging of the estrous cycle using stained vaginal. *Toxicologic pathology*.
8. Hubscher, C. B. (2005). A quantitative method for assessing stages of rat estrous cycle. *Biotechnic & histochemistry : official publication of the Biological Stain Commission*, 79-87.
9. Pantier, L. L. (2019). Estrous cycle monitoring in mice with rapid data visualization and analysis. *Bio-Protocol*.
10. Hernandez Hernandez, G. D.-M.-A.-C.-L. (2019). Estrous cycle classification through automatic feature extraction. Computacion y Sistemas , 1249-1259.
11. Sano, K. M. (2020). Deep learning-based classification of the mouse estrous cycle stages. Scientific Reports.
12. Pessoa LFC and Maragos P (2000). "Neural networks with hybrid morphological/rank/linear nodes: a unifying framework with applications to handwritten character recognition.", Pattern Recognition 33:945–960.
13. Araújo RA and Sussner P (2010). "An increasing hybrid morphological-linear perceptron with pseudo gradient-based learning and phase adjustment for financial time series prediction.", in: Proceed ings of the 2010 IEEE World Congress on Computational Intelligence, Vol. IJCNN, Barcelona, Spain, pp. 807–814.
14. Arce F et al.(2019). "Dendrite Ellipsoidal Neuron Trained by Stochastic Gradient Descent for Motor Imagery Classification.", In: Carrasco-Ochoa J., Martínez-Trinidad J., Olvera-López J., Salas J. (eds) Pattern Recognition. MCPR 2019.: Lecture Notes in Computer Science, vol 11524. Springer, Cham.
15. Ritter GX et al. (2003). "Morphological perceptrons with dendritic structure." ,In: The 12th IEEE International Conference on Fuzzy Systems, FUZZ 2003, Volume 2, 1296-1301.
16. Arce F et al. (2017). "Dendrite Ellipsoidal Neuron", In: 2017 International Joint Conference on Neural Networks (IJCNN), Anchorage, AK, pp. 795-802.
17. Gómez-Flores, Wilfrido & Sossa, Humberto. (2021). Improving the Classification Performance of Dendrite Morphological Neurons. IEEE transactions on neural networks and learning systems. PP. 10.1109/TNNLS.2021.3116519.
18. RitterGXand UrcidG(2007). "Learning in Lattice Neural Networks that Employ Dendritic Computing.", In: Kaburlasos V.G., Ritter G.X. (eds) Computational Intelligence Based on Lattice Theory. Studies in Computational Intelligence 2007, vol 67. Springer, Berlin, Heidelberg.
19. Hernández G et al. (2018). "Morphological-Linear Neural Network", 2018 IEEE International Conference on Fuzzy Systems (FUZZ-IEEE), Rio de Janeiro, pp. 1-6.
20. Román Godínez, R. F., Zamora, E., & Sossa, H. (2021). A Comparative Study of Dendrite Neural Networks for Pattern Classification. International Journal of Combinatorial Optimization Problems and Informatics, 12(3), 8-19.
21. Szeliski, R. (2011). Computer Vision. Algorithms and Applications. London: Springer-Verlag.
22. Ochoa-Montiel, R. O. (2020). Expert knowledge for the recognition of leukemic cells. Appl. Opt., 4448-4460.
23. Gómez-Flores, W. S. (2021). Smooth dendrite morphological neurons. Neural Networks, 40-53.
24. Sossa, Humberto & Virgilio González, Carlos. (2022). Spiking neural networks and dendrite morphological neural networks: an introduction. 10.1016/B978-0-12-820125-1.00022-1.
25. Gómez-Flores W and Sossa JH (2020), "Towards Dendrite Spherical Neurons for Pattern Classification", In: Figueroa Mora K., Anzurez Marín J., Cerda J., Carrasco-Ochoa J., Martínez-Trinidad J., Olvera-López J. (eds) Pattern Recognition, MCPR 2020. Lecture Notes in Computer Science, vol 12088. Springer, Cham.
26. L. Delgado *et al*. (2017). "Classification of the estrous cycle through texture and shape features," *2017 IEEE Symposium Series on Computational Intelligence (SSCI)*, pp. 1-7, doi: 10.1109/SSCI.2017.8285390.
27. Clausi, D. (2002). An analysis of co-occurrence texture statistics as a function of grey level quantization. *Canadian Journal of Remote Sensing*.
28. Breiman, L. (2001). Random Forests. *Machine Learnings*, 5-32.